Experimental study of the diffracted wave pattern around a fast displacement vessel

C. Lugni, M. Landrini, M. Ohkusu* and *F. La Gala*

INSEAN, *The Italian Ship Model Basin*, Roma, Italy. maulan@waves.insean.it
$\star$ RIAM, *Kyushu University*, Fukuoka, Japan.

Introduction

There is a large interest in the development of numerical tools to predict loads and motions of a ship in waves. For most of these methods, verification and validation are usually provided by measured response amplitude operators. Such global data are not necessarily indicative of the actual accuracy of the considered solver because, often, the ship behavior is determined by the gross fluid dynamics involved, which can be captured reasonably well by several methods presently available. On this ground, the availability of local data is a valuable support for developing numerical techniques to describe the flow field around a ship in waves.

From a more fundamental point of view, wave-body interaction is by no means a phenomenon fully understood and described. The elementary physics is well interpreted by the linear-scattering theory but the actual observation of the flow around the bow of a ship sailing through waves shows the extremely rich and complex fluid-flow phenomena.

In this framework, we are pursuing a theoretical-numerical and experimental investigation aimed to give a more complete description of the wave pattern around a ship sailing through regular waves.

We have selected the Model 5415 of the DTMB which is representative of a class of frigates, with slender hull, sharp stem, and relatively fast operation speed. For this hull form a large set of reference data are available for the steady-wave pattern [7] and the scope of the activity is to provide wave data for the unsteady case. A preliminary set of seakeeping tests have been already developed to get confidence with the behaviour of such ship in waves, [2].

Experimental Method and Analysis

The main tool of our experimental investigation is the unsteady wave-pattern analysis (UWPA) introduced by Ohkusu [4, 5, 6]. The key idea is to assume a mathematical structure for the unsteady wave field $\eta(P,t)$ around the ship of the form

$$\eta(P,t) = \eta_0(P) + \sum_k \eta_k(P) e^{ik\omega t} \ . \qquad (1)$$

Here, $\eta_0(P)$ is the mean wave pattern, while the remaining terms are the components oscillating with the frequency of encounter ω and its multiples. In case of calm-water tests, $\eta_0(P)$ is the steady wave pattern. This is not anymore true in presence of incident waves since nonlinear interaction effects between oscillating components imply a contribution with non-zero mean.

This analysis allows the identification of the terms entering in (1). In details, *cf.* fig. 1, the method is based on using an array of fixed wave probes, uniformly spaced along the longitudinal direction of the towing tank and at a specified distance from the ship center-plane. During the test, each wave gauge records the free-surface elevation in the towing-tank reference frame. To reconstruct the wave elevation $\eta(P,t)$ relative to an observer moving with the ship model, we collect the samples from all the wave probes corresponding to the time instant when the observer is passing through each wave-probe location. The time interval between two successive samples is the time needed for the observer to move from one gauge to the next one, *i.e.* $\Delta t = \Delta x/U$. Therefore, in this analysis, the longitudinal spatial resolution depends on the sampling rate of the wave elevation measurements, while the distance Δx among the wave gauges defines the time resolution $\Delta x/U$ in the frame of reference moving with the ship model. The frequency components of the reconstructed time history $\eta(P,t)$ are identified by standard Fourier analysis. In the present experiment, we adopted twenty wave probes and the Fourier analysis has been performed up to the third harmonic component.

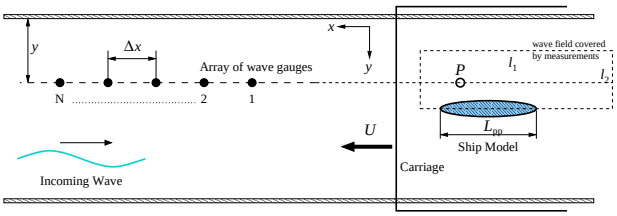

Fig. 1: Sketch of the experimental set up and main symbols adopted.

The proposed investigation differs from that presented in [3], where the linear-diffraction wave field is deduced from the total wave elevation by subtracting the incident wave field and the measured mean wave elevation.

Set up

The tests have been carried out at INSEAN towing tank No.2 (length: 220 m, breadth: 9 m, depth: 3.6 m). Regular waves have been generated by a flap-type wavemaker hinged at 1·8 m above the tank bottom. The wave maker is controlled by a computer and provides a good quality of the waves within the frequency range 0·1–1·3 Hz. A wooden beach with a parabolic shape ensure a contribution of the reflected waves less than 7%, within the specified frequency range.

A model similar to Model 5415 of DTMB [1] has been towed restrained to move and kept in even keel condition. The geometrical scale is 24·824, and the actual length of the model is $L_{pp} = 5{\cdot}72$ m.

The investigated wave field around the model (see fig. 1) is $\ell_1 \sim 2{\cdot}5L_{pp}$ long in the longitudinal direction and $\ell_2 = 0{\cdot}5L_{pp}$ wide in the transverse direction. The considered Froude number is Fr$= 0{\cdot}269$, and regular waves in the range $\lambda/L_{pp} = 0{\cdot}5, 0{\cdot}75$ are adopted.

Nonlinear effects are investigated by increasing the wave steepness: $kA = 0{\cdot}05, 0{\cdot}1, 0{\cdot}2$. According to the selected wavelength, the transverse spacing on the free-surface grid varies in the range $\delta/L_{pp} = 1/80 - 1/60$.

For the measurements, home-developed capacitance wave gauges have been adopted. To reduce noise and avoid phase errors, a miniaturized driving/acquisition hardware was located on top of the wave wire and equipped with an on-board memory able to record the measured data. These have been downloaded at the end of each test. The sampling rate was 50 Hz. Twenty wave probes were fixed equally spaced along a motorized arm, which is shifted transversally after each run.

By an error-source analysis, it was found that the accuracy of the measurements is dominated by the precision of the wave probes. The latter is of order of 1 mm.

Numerical computations

The experimental analysis will be complemented by numerical simulations. A frequency-domain approach has been adopted to solve for the three-dimensional diffraction problem. In the method, the problem is linearized around the double-body flow and recast into integral form by a source formulation. Flat panels, with piecewise-constant source strength are used to discretized the boundary domain and the integral equations. An example of computations is given later in the discussion. Also an investigation by means of 2.5D (or 2D+t) theory for fast and slender ships will be performed to gain further information on the role of nonlinearities. A mixed Eulerian-Lagrangian method based on boundary integral equations will be used to solve numerically the related problem.

Preliminary observations

Figures 2-4 present the analyzed results for $\lambda/L = 0{\cdot}5$ and increasing steepness, $kA = 0{\cdot}05$, $0{\cdot}1$ and $0{\cdot}2$, respectively.

In each figure, the top plot shows the mean component deduced from UWPA compared with the steady wave field obtained by testing the model in calm water. As we can see, for the smallest steepness the two wave fields are in reasonable agreement. We note that, for this model scale and the selected Froude number, wave-breaking phenomena are not visible both in calm-water tests and during tests in waves. As the wave steepness increases, the mean component obtained by UWPA diverges progressively with respect to the wave pattern in calm water. In particular, in the former the divergent bow wave is "attenuated" with respect to the calm-water case. On the contrary, the waves down the transom stern are larger, especially for $kA = 0{\cdot}2$. Both for bow and for stern waves, the crests form a larger angle with respect to the longitudinal direction. This could be connected with periodic wave-breaking phenomena visible during the passage of the ship bow through the wave crest. The photographic sequence in Fig. 5 shows one breaking cycle for $kA = 0{\cdot}2$.

For the considered kA, the ω, 2ω and 3ω components of the diffracted wave patter are shown respectively in second to fourth plots of figures 2-4. The incident wave field is not shown. The upper (lower) portion of each line-contour diagram gives the real (imaginary) part of the corresponding harmonic component.

As expected, the third harmonics are those more significantly affected by the accuracy of the measurements. In particular, for $kA = 0{\cdot}05$, *cf.* figure 2, the presence of a definite wave pattern can hardly be detected and just a sort of "shadow" behind the hull can be seen. The signal-to-noise ratio increases as the steepness increases and clearer results, even at third order, can be seen for larger steepnesses.

For all the components, the qualitative structure of the observed wave pattern is consistent with the physical intuition: the wave crests are distributed inside a V-shaped region and curved ahead in the forward direction. Clearly, the wavelength is shorter for the higher harmonics.

For $kA = 0{\cdot}05$, figure 6 shows the comparison between the numerical solution of the linearized diffraction problem and the present measurements. The overall pattern is in qualitative agreement. The numerically predicted peak values along the ship centerline are larger than the experimental ones, while those observed near the V-shaped domain are of the same order. This difference is visible both along and downstream the hull. We are still speculating the possible origin of this discrepancy.

As the wave steepness increases, the first Fourier component decreases relative to the higher ones. This is emphasized by the chosen scaling, where the amplitude of the n-component is divided by $(kA)^n$. With these premises, as kA increases, the amplitudes of the 2ω and 3ω components increase at the expense of the ω component. By comparing the results for $kA = 0{\cdot}1$ and $kA = 0{\cdot}2$, we observe that the 2ω is also decreasing as the steepness increases showing a sort of saturation effect of the lower Fourier components in favor of the higher ones as the nonlinearities of the phenomenon are larger.

A fuller discussion of the data will be given at the Workshop.

References

[1] http://www50.dt.navy.mil/5415/geom.html

[2] A. Colagrossi, C. Lugni, M. Landrini, G. Graziani (2001) Numerical and experimental transient tests for ship seakeeping. Int. J. Polar Off. Engng.

[3] L. Gui, J. Long, B. Metcalf, J. Shao, F. Stern (2000) Forces, moment and wave pattern for naval combatant in regular head waves. 23^{rd} Symp. on Naval Hydrodynamics, Rouen (France).

[4] M. Ohkusu, G. Wen (1996) Radiation and diffraction waves of a ship at forward speed. 21^{st} Symp. on Naval Hydrod., Trondheim (Norway).

[5] M. Ohkusu (1998) Validation of Theoretical Methods for Ship Motions by Means of Experiment. 22^{nd} Symp. on Naval Hydrod., Washington (USA).

[6] M. Ohkusu, M. Yasunaga (2000) Second order waves generated by ship motions. 23^{rd} Symp. on Naval Hydrod., Rouen (France).

[7] F. Stern, J. Long, R. Penna, A. Olivieri, T. Ratcliff, H. Coleman (2000) International collaboration on benchmark CFD validation data for naval surface combatant. 23^{rd} Symp. on Naval Hydrodynamics, Rouen (France)

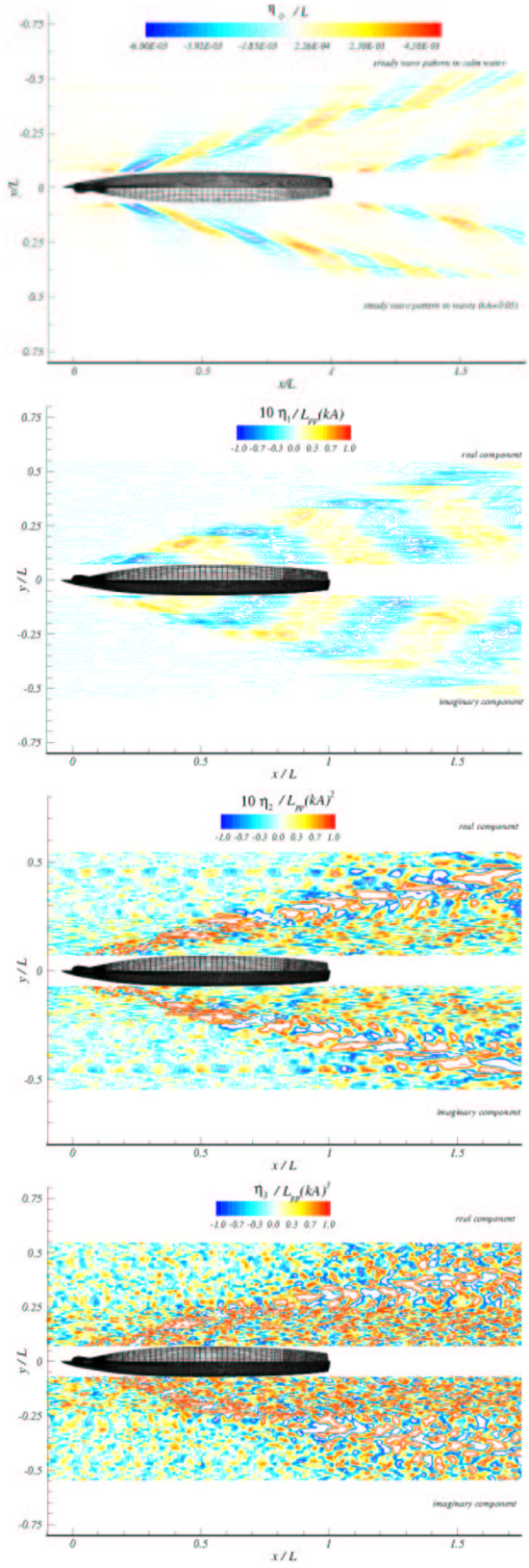

Fig. 2: Unsteady wave pattern for $kA = 0{\cdot}05$, $\lambda/L = 0{\cdot}5$. From top to bottom: comparison between the measured mean wave pattern and the steady component of the wave field; first Fourier component; second Fourier component; third Fourier component.

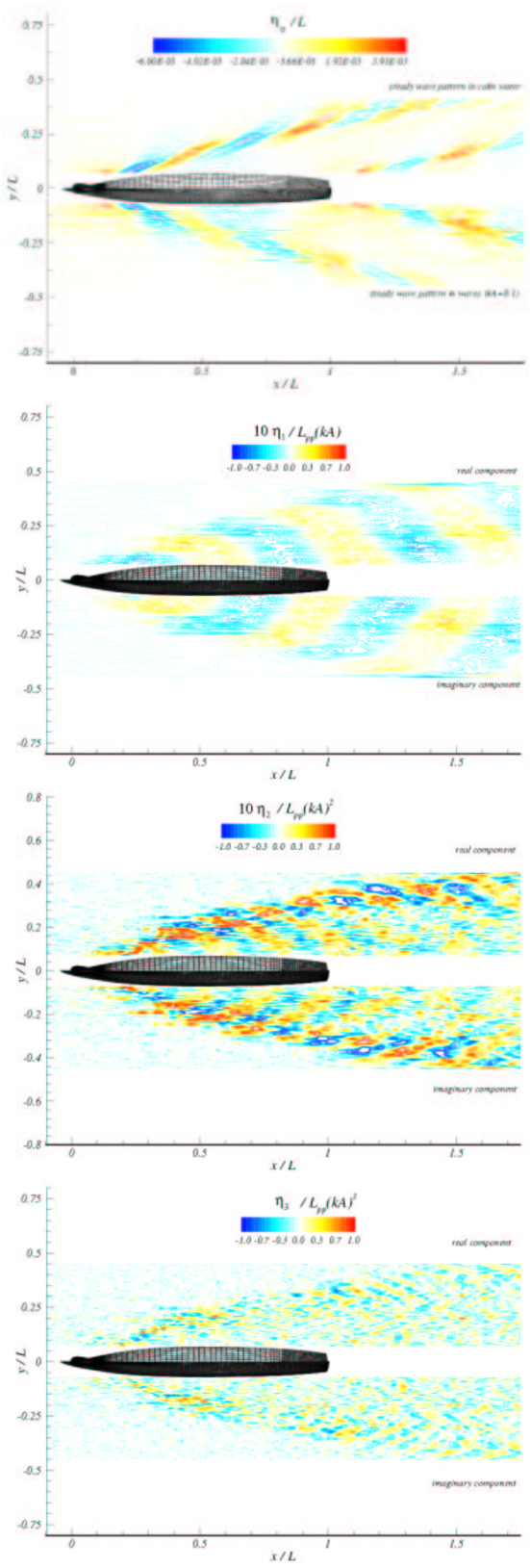

Fig. 3: Unsteady wave pattern for $kA = 0{\cdot}1$, $\lambda/L = 0{\cdot}5$. From top to bottom: comparison between the measured mean wave pattern and the steady component of the wave field; first Fourier component; second Fourier component; third Fourier component.

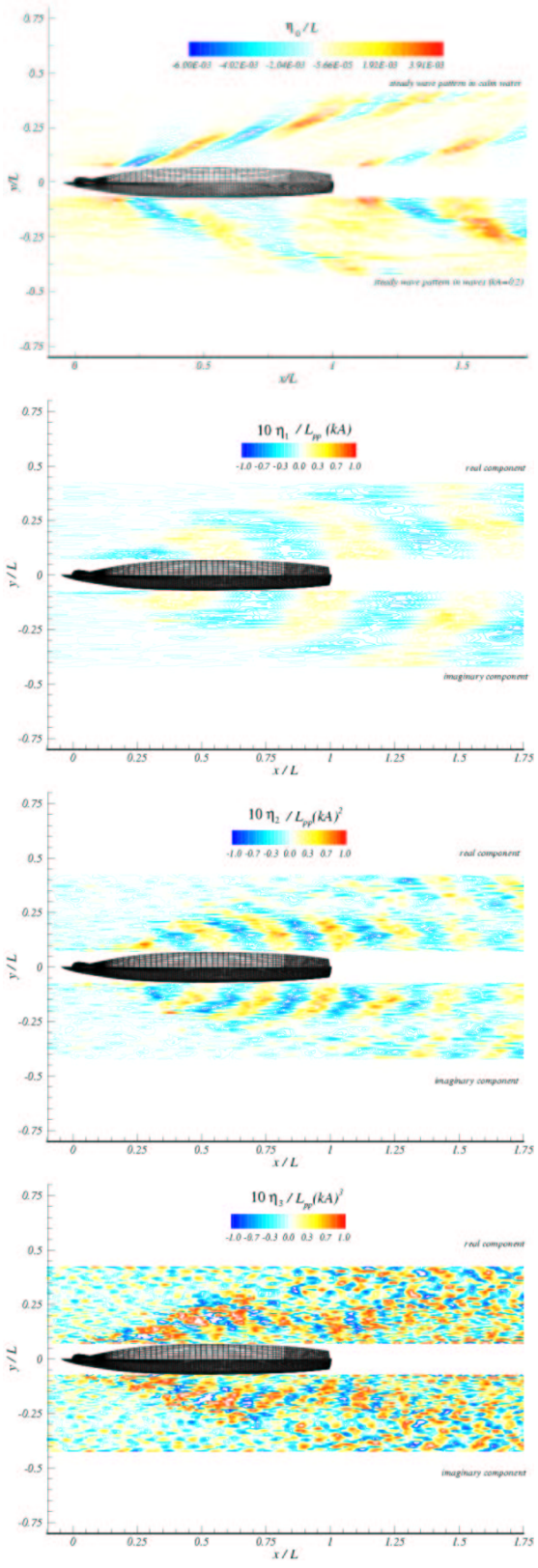

Fig. 4: Unsteady wave pattern for $kA = 0{\cdot}2$, $\lambda/L = 0{\cdot}5$. From top to bottom: comparison between the measured mean wave pattern and the steady component of the wave field; first Fourier component; second Fourier component; third Fourier component.

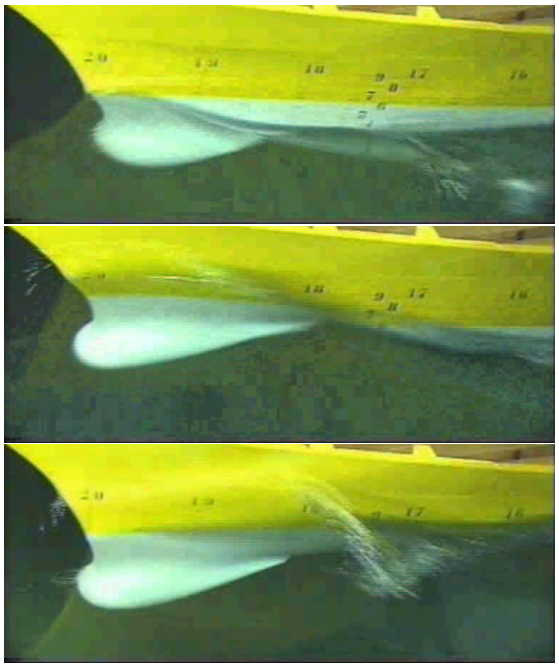

Fig. 5: Phases of the cyclical wave breaking at the bow during the ship passage through the wave crest. The interval between the pictures is 0·34 the period of encounter. Top: the bow has just passed the wave trough. The divergent wave similar to that of the steady wave pattern in calm water is visible. Center: the bow stem has reached the wave crest. A jet is formed at the hull and starts falling down against the free surface. Bottom: impact of the plunging jet against the free surface.

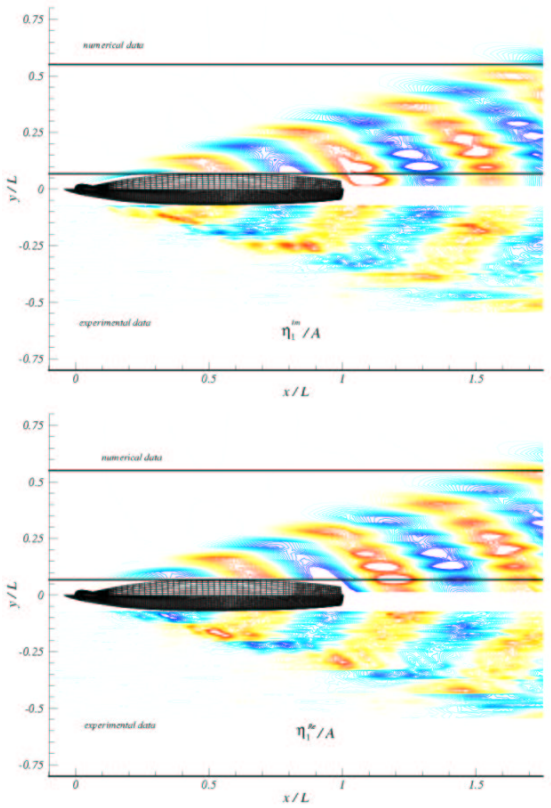

Fig. 6: Unsteady wave pattern for $kA = 0{\cdot}05$, $\lambda/L = 0{\cdot}5$. Comparison between the measured first Fourier component and linearized numerical computations. Top: imaginary part. Bottom: real part.